AAS 10-209

# CALIBRATION TECHNIQUE FOR ATTITUDE MANOEUVRES OF SPINNING SATELLITES

Jozef C. van der Ha*

The paper presents an efficient practical calibration technique for rhumb-line attitude control manoeuvres of spin-stabilized satellites. The only measurements used in the calibrations are the solar aspect angles generated by a common V-slit Sun sensor. Both the path-length and rhumb-line angle can be established accurately by using the initial and final Sun aspect angles of two independent manoeuvre paths. This technique was applied successfully for the CONTOUR mission in summer 2002 before executing a full 180-deg flip manoeuvre. The final attitude error at the end of the manoeuvre was below 3 deg in arc-length.

## INTRODUCTION

We present an efficient and practical calibration technique for rhumb-line attitude control manoeuvres of spin-stabilized satellites. The calibration technique requires only measurements produced by a V-slit Sun sensor. It has actually been employed successfully during the initial operations of the CONTOUR mission in its Earth-orbiting phase in July 2002. This technique can easily be implemented and may therefore be of interest to other satellites as well.

A 180-deg attitude reorientation manoeuvre needed to be performed a few days after CONTOUR's separation from the launcher[1]. At that time, the hydrazine thrusters that were to be used for this manoeuvre had not been calibrated. In fact, they had not even been used. Therefore, there was a significant risk that the satellite attitude would not be able to reach its final target attitude with the necessary precision of only 'a few degrees' (due to system-level requirements).

The attitude control of a spin-stabilized spacecraft can be accomplished by a forced precession of the spin axis. In practice, this is accomplished by a sequence of thrust pulses (by one or more thrusters) that are synchronized with the spin phase angle (see References 2 - 3 for more details).

The inertial direction of the spin-axis motion can be controlled by introducing a constant delay time in the start of the thruster firings relative to the instant when the Sun crosses the Sun sensor's vertical slit. This strategy makes the spin-axis direction follow a rhumb-line path as illustrated in Figure 1. The angle $\chi$ is the constant rhumb angle relative to the *Sun cone* (i.e., the local latitude circle) on the unit-sphere with the Sun at the north-pole location.

The manoeuvre path-length $\lambda_f$ is proportional to the number and magnitude of the applied thrust pulses. Therefore, any errors in the intended thrust level or in the number of desired thrust pulses lead to errors in the resulting total path-length.

* Professor, Department of Aeronautics & Astronautics, Kyushu University, 744 Motooka, Nishi-ku, Fukuoka 819-0395, Japan.

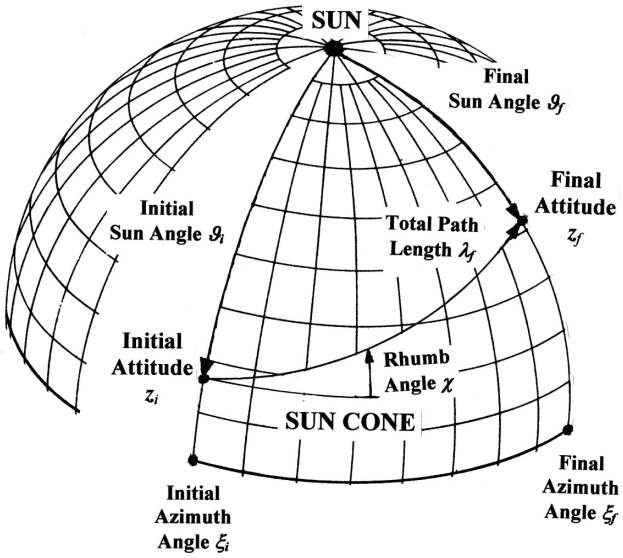


**Figure 1 – Spherical Geometry of Rhumb-Line Manoeuvre**

It may be noted that the rhumb-line path length is in general different from the corresponding minimum great-circle arc-length distance between the initial and final attitude vectors. In practice, however, it is usually fairly close, especially for small manoeuvres (see Reference 2).

The second parameter defining the manoeuvre path is the rhumb angle $\chi$ shown in Figure 1. This angle represents the sum of the delay angle of the initiation of the thrust pulses (relative to the instant of the Sun crossing the Sun sensor vertical slit) and the centroid or mid-time of the thrust pulses. Furthermore, the offset between the Sun-sensor position and the thruster location(s) within the satellite's body reference frame must be taken into account in the calculation of $\chi$. Errors in any of these input parameters lead to proportional errors in the effective rhumb angle.

## MANOEUVRE CALIBRATION PARAMETERS

### Mathematical Formulation

The mathematical formulation employed here is based on the rhumb-line model established in Eqs. (29) of Reference 2. This model makes careful distinctions between the independent and dependent variables:

$$\vartheta_f(\vartheta_i, \lambda_f, \chi) = \vartheta_i - \lambda_f \sin\chi \tag{1a}$$

$$\xi_f(\xi_i, \vartheta_i, \lambda_f, \chi) = \xi_i - \left\{ y(\vartheta_f) - y(\vartheta_i) \right\} / \tan\chi \tag{1b}$$

The logarithmic function $y(\vartheta)$ is defined by:

$$y(\vartheta) = \ell n\{\tan(\vartheta/2)\} \tag{1c}$$

The expression for the variable $\xi_f$ in Eq. (1b) contains hidden dependencies because $\vartheta_f$ is a function of the independent variables $\vartheta_i$, $\lambda_f$, and $\chi$ as indicated by Eq. (1a). Equations (1) provide a useful model for analyzing the error propagations over the manoeuvre path (see Reference 2). The same system of equations will be used here for establishing the calibration scheme.

The variables appearing in Eqs. (1) represent those belonging to the *actual* rhumb-line manoeuvre path. Therefore, $\vartheta_i$ and $\vartheta_f$ refer to the *actual* values of the initial and final Sun aspect angles, respectively. Similarly, $\lambda_f$ and $\chi$ are the *actual* path-length and rhumb angle. It must be noted that, in practice, these actual variables remain unknown during the manoeuvre planning, during the manoeuvre execution, as well as during its evaluation.

**Planned Manoeuvre Parameters**

The *planned* manoeuvre is designed and prepared prior to the actual manoeuvre execution. The equations describing the planned manoeuvre employ the same rhumb-line model as in Eqs. (1) with the understanding that it now contains the *planned* parameters, i.e. $\vartheta_{i,p}$, $\vartheta_{f,p}$, $\lambda_{f,p}$, and $\chi_p$. In particular, the counterpart of Eq. (1a) can be written as:

$$\vartheta_{f,p}(\vartheta_{i,p}, \lambda_{f,p}, \chi_p) = \vartheta_{i,p} - \lambda_{f,p} \sin \chi_p \tag{2}$$

We focus now on the differences between the actual and planned manoeuvre parameters and introduce the associated small *difference parameters*, i.e. $\Delta a = a - a_p$:

$$\Delta\vartheta_i = \vartheta_i - \vartheta_{i,p};\ \Delta\vartheta_f = \vartheta_f - \vartheta_{f,p};\ \Delta\lambda_f = \lambda_f - \lambda_{f,p};\ \Delta\chi = \chi - \chi_p \tag{3}$$

When subtracting the expressions in Eq. (1a) and Eq. (2) we obtain:

$$\Delta\vartheta_f = \Delta\vartheta_i + \lambda_{f,p} \sin \chi_p - \lambda_f \sin \chi \tag{4}$$

This expression can be simplified by means of a Taylor-series expansion of the final term about the known parameters $\lambda_{f,p}$ and $\chi_p$. Finally, we obtain the approximate first-order result:

$$\Delta\vartheta_f \approx \Delta\vartheta_i - \left(\sin \chi_p\right)\Delta\lambda_f - \left(\lambda_{f,p} \cos \chi_p\right)\Delta\chi \tag{5}$$

**Measured Manoeuvre Parameters**

During the in-flight manoeuvre execution, the Sun sensor produces the measurements of the start and end values of the solar aspect angles, i.e. the angles $\vartheta_{i,m}$ and $\vartheta_{f,m}$. When including the respective random noise contributions $m_i$ and $m_f$, we can construct relationships between the *measured* Sun aspect angles $\vartheta_{i,m}$ and $\vartheta_{f,m}$ and the *actual* rhumb-line parameters $\lambda_f$ and $\chi$ of Eq. (1a) as follows:

$$\vartheta_{i,m} = \vartheta_i + m_i;\ \ \vartheta_{f,m} = \vartheta_f + m_f \ \ \Rightarrow \tag{6a,b}$$

$$\vartheta_{f,m} - \vartheta_{i,m} = -\lambda_f \sin \chi + m \tag{6c}$$

The noise term $m = m_f - m_i$ represents the difference between the random errors in the final and initial Sun-aspect-angle measurements of Eqs. (6a,b). It can be seen that identical biases in the two Sun-angle measurements would cancel by the subtraction in Eq. (6c). Differential bias errors, however, would affect the result of Eq. (6c) but they are expected to be minor so we may ignore them here. Furthermore, we assume that the random noise terms $m_f$ and $m_i$ are independent and have vanishing expected values, i.e. $E\{m_f\} = E\{m_i\} = 0$.

In summary, we have the following statistical properties of the noise term $m$:

$$E\{m\} = E\{m_f - m_i\} = E\{m_f\} - E\{m_i\} = 0 \tag{7a}$$

$$E\{m^2\} = E\{m_f^2\} + E\{m_i^2\} = 2E\{\vartheta^2\} = 2\sigma_\vartheta^2 \tag{7b}$$

where $\sigma_\vartheta^2$ denotes the expected variance of the individual Sun-aspect-angle measurements. When ignoring nutation effects, the standard deviation $\sigma_\vartheta$ of the measurement noise in the Sun aspect angle in Eq. (7b) is typically of the order of only 0.001 deg (see Reference 4).

Now we introduce the notation $\delta a = a_m - a_p$ for the difference between the *measured* and *planned* parameters, i.e. $a_m$ and $a_p$, of an arbitrary unknown variable $a$. When subtracting the measured and the planned final solar aspect angles in Eqs. (6c) and (2), respectively, we find:

$$\begin{aligned}\delta\vartheta_f &= \vartheta_{f,m} - \vartheta_{f,p} = \vartheta_{i,m} - \lambda_f \sin\chi + m - \left(\vartheta_{i,p} - \lambda_{f,p}\sin\chi_p\right) = \\ &= \delta\vartheta_i - \lambda_f \sin\chi + \lambda_{f,p}\sin\chi_p + m \approx \\ &\approx \delta\vartheta_i - \left(\sin\chi_p\right)\Delta\lambda_f - \left(\lambda_{f,p}\cos\chi_p\right)\Delta\chi + m \end{aligned} \tag{8}$$

The $\Delta$ symbol appearing in Eq. (8) has been defined in Eq. (3) and refers to the differences between actual and planned manoeuvre variables.

It is of interest to compare the result of Eq. (8) with Eq. (5) which looks very similar. Eq. (5) deals with the differences between the unknown actual manoeuvre parameters and the associated planned parameters. Eq. (8), on the other hand, relates the planned manoeuvre variables to the measured ones, which forms the basis for the calibration strategy to be discussed next.

Figure 2 provides an illustration of the rhumb-line variables and Sun-angle differences.

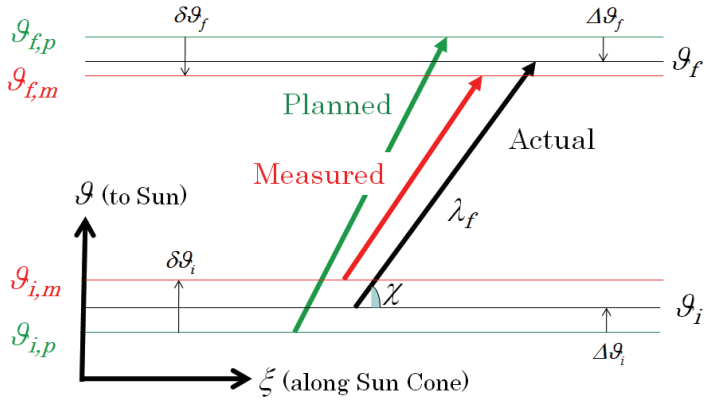


**Figure 2 – Visualization of Manoeuvre Parameters and their Differences**

## COMPUTATION OF CALIBRATION PARAMETERS

### Rhumb-Line Calibration Equations

In practical applications, the Sun Sensor produces much more accurate measurements than for instance the infra-red horizon Earth sensors (in terms of random errors and biases). Therefore, it is advantageous to perform the calibration procedure based on Sun sensor measurements only.

When considering a single manoeuvre path, we find that Eq. (8) provides only *one* equation for the *two* unknown errors $\Delta\lambda_f$ and $\Delta\chi$. Therefore, the initial and final Sun angle measurements $\vartheta_i$ and $\vartheta_f$ cannot achieve the immediate calibration of *both* rhumb-line parameters $\lambda$ and $\chi$.

Therefore, we propose a strategy that uses two separate manoeuvre paths to achieve the calibrations of both rhumb-line parameters using only Sun-aspect-angle measurements. The two paths must have different rhumb angles to provide two independent equations for the two unknowns. In general, with the help of Eq. 8, we can write the two manoeuvre path equations as:

$$\delta\vartheta_f^{(1)} - \delta\vartheta_i^{(1)} = -\left(\sin\chi_p^{(1)}\right)\Delta\lambda_f^{(1)} - \left(\lambda_{f,p}^{(1)}\cos\chi_p^{(1)}\right)\Delta\chi^{(1)} + m^{(1)} \tag{9a}$$

$$\delta\vartheta_f^{(2)} - \delta\vartheta_i^{(2)} = -\left(\sin\chi_p^{(2)}\right)\Delta\lambda_f^{(2)} - \left(\lambda_{f,p}^{(2)}\cos\chi_p^{(2)}\right)\Delta\chi^{(2)} + m^{(2)} \tag{9b}$$

where the superscripts (1) and (2) designate each of the two individual manoeuvre paths.

As long as the manoeuvres are performed by the same thrusters(s) and if the effects of propellant blow-down and other time-dependent effects can be considered negligible, the ratios $\Delta\lambda^{(1)} / \lambda_{f,p}^{(1)}$ and $\Delta\lambda^{(2)} / \lambda_{f,p}^{(2)}$ will be identical. Similarly, when assuming identical conditions for the thrust centroid time and other timing parameters during both manoeuvre paths, we can assume that also the rhumb-line errors $\Delta\chi^{(1)}$ and $\Delta\chi^{(2)}$ will be identical.

We can simplify Eqs. (9) by introducing the abbreviations:

$$y_j = \left(\delta\vartheta_f^{(j)} - \delta\vartheta_i^{(j)}\right) / \lambda_{f,p}^{(j)}, \quad j = 1,2 \tag{10a}$$

$$x_1 = \Delta\lambda_f^{(1)} / \lambda_{f,p}^{(1)} = \Delta\lambda_f^{(2)} / \lambda_{f,p}^{(2)}; \quad x_2 = \Delta\chi^{(1)} = \Delta\chi^{(2)} \tag{10b,c}$$

$$a_{j1} = -\sin\chi_p^{(j)}; \quad a_{j2} = -\cos\chi_p^{(j)}, \quad j = 1, 2 \tag{10d,e}$$

$$m_j = m^{(j)} / \lambda_{f,p}^{(j)}, \quad j = 1, 2 \tag{10f}$$

The parameter $x_1$ represents the calibration coefficient or scale factor of the manoeuvre path-length and the parameter $x_2$ is the calibration constant of the rhumb angle in radians.

Finally, we write the system of Eqs. (9) in the compact vector-matrix form:

$$\mathbf{y} = \begin{pmatrix} y_1 \\ y_2 \end{pmatrix} = \begin{bmatrix} a_{11} & a_{12} \\ a_{21} & a_{22} \end{bmatrix} \begin{pmatrix} x_1 \\ x_2 \end{pmatrix} + \begin{pmatrix} m_1 \\ m_2 \end{pmatrix} = A\mathbf{x} + \mathbf{m} \tag{11}$$

The noise terms $m^{(j)}$ for $j = 1, 2$ are in general very small because of the accurate Sun-sensor readings as discussed below Eq. (7). Furthermore, the definition of the noise terms $m_j$ ($j = 1, 2$) in Eq. (10f) shows that the noise effect decreases when increasing the manoeuvre path-length $\lambda_f$.

**Solutions for Calibrated Parameters**

When ignoring, for the time being, the noise term **m** and assuming that the matrix $A$ is non-singular, we can immediately solve for the unknown parameters $x_j$ ($j = 1, 2$) in Eq. (11):

$$\mathbf{x} = \begin{pmatrix} x_1 \\ x_2 \end{pmatrix} = A^{-1} \begin{pmatrix} y_1 \\ y_2 \end{pmatrix} = A^{-1}\mathbf{y} \tag{12}$$

with the inverse matrix $A^{-1}$ given by:

$$A^{-1} = \frac{1}{a_{11}a_{22} - a_{12}a_{21}} \begin{bmatrix} a_{22} & -a_{12} \\ -a_{21} & a_{11} \end{bmatrix} \tag{13}$$

We calculate the elements of the matrix $A^{-1}$ in explicit terms of the elements of the matrix $A$ defined in Eqs. (10d,e):

$$A^{-1} = \frac{1}{\sin\left(\chi_p^{(2)} - \chi_p^{(1)}\right)} \begin{bmatrix} \cos\chi_p^{(2)} & -\cos\chi_p^{(1)} \\ -\sin\chi_p^{(2)} & \sin\chi_p^{(1)} \end{bmatrix} \tag{14}$$

Finally, we obtain the explicit results for the calibration parameters from Eqs. (10) to (14):

$$x_1 = \frac{1}{\sin\left(\chi_p^{(2)} - \chi_p^{(1)}\right)} \left\{ \frac{\left(\delta\vartheta_f^{(1)} - \delta\vartheta_i^{(1)}\right)}{\lambda_{f,p}^{(1)}} \cos\chi_p^{(2)} - \frac{\left(\delta\vartheta_f^{(2)} - \delta\vartheta_i^{(2)}\right)}{\lambda_{f,p}^{(2)}} \cos\chi_p^{(1)} \right\} \tag{15a}$$

$$x_2 = \frac{1}{\sin\left(\chi_p^{(2)} - \chi_p^{(1)}\right)} \left\{ -\frac{\left(\delta\vartheta_f^{(1)} - \delta\vartheta_i^{(1)}\right)}{\lambda_{f,p}^{(1)}} \sin\chi_p^{(2)} + \frac{\left(\delta\vartheta_f^{(2)} - \delta\vartheta_i^{(2)}\right)}{\lambda_{f,p}^{(2)}} \sin\chi_p^{(1)} \right\} \tag{15b}$$

We note that a singularity occurs when the two rhumb angles of the two manoeuvre paths are equal or differ by +/- 180 deg. In these situations, the two equations are *not* independent and unambiguous solutions for the calibration parameters $x_1$ and $x_2$ cannot be established. In these cases, at least one different manoeuvre path should be selected for achieving the calibrations.

**Orthogonal Manoeuvre Paths**

The following four special cases are of considerable practical interest:

$$\chi_p^{(1)} = \pm 90°; \quad \chi_p^{(2)} = 0 \text{ or } 180° \tag{16a,b}$$

Each of the four pairs of rhumb angles( $\chi_p^{(1)}, \chi_p^{(2)}$ ) represents two successive orthogonal manoeuvre paths. For example, we take the pair (+ 90°, 0) and find the simplified results of Eqs. (15):

$$x_1 = \Delta\lambda_f^{(1)} / \lambda_{f,p}^{(1)} = -\left(\delta\vartheta_f^{(1)} - \delta\vartheta_i^{(1)}\right) / \lambda_{f,p}^{(1)} \tag{17a}$$

$$x_2 = \Delta\chi^{(2)} = -\left(\delta\vartheta_f^{(2)} - \delta\vartheta_i^{(2)}\right) / \lambda_{f,p}^{(2)} \tag{17b}$$

Similar results (with different signs) can be established for the other three pairs in Eqs. (16).

Finally, we convert the results of Eqs. (17) into the *calibrated* (i.e., *updated*) parameters $\lambda_{f,c}$ and $\chi_c$ for each of the two planned manoeuvre paths as follows:

$$\lambda_{f,c}^{(1)} = \lambda_{f,p}^{(1)} + \Delta\lambda_f^{(1)}; \quad \chi_c^{(2)} = \chi_p^{(2)} + \Delta\chi^{(2)} \tag{18a,b}$$

These results form the basis for calibrating the thrust level and the thrust centroid time, respectively, which may then be used in the preparation of future manoeuvres. In particular, the thrust-level calibration is given by:

$$T_c = \left(1 + \Delta\lambda_f^{(1)} / \lambda_{f,p}^{(1)}\right) T_p \tag{19}$$

where $T_p$ and $T_c$ denote the planned and calibrated thrust levels, respectively. Because spin-rate changes affect the delay angle between the Sun-sensor signal and the start of the thrust pulses, care should be taken to eliminate their effects from the centroid time calibrations.

The specific pairs of manoeuvre paths in Eqs. (16) have the attractive property that the calibrations of the path-length and the rhumb angle are strictly separated in the two manoeuvre paths.

During the first path with planned rhumb angle $\chi_p = +90°$, the spin axis moves nominally straight towards the Sun position in inertial space, as can be visualized with the help of Figure 1. We see that the Sun aspect angle decreases continuously over the manoeuvre path. If the measured final Sun aspect angle is larger than the planned final Sun aspect angle we can conclude that the thrust-level underperformed.

Thus, the thrust level will be assigned a negative calibration, which is consistent with the minus sign in Eq. (17a). In this case, the measurements of the Sun aspect angle at the start and end of the manoeuvre path provide accurate information on the actually achieved path-length, which enables us to perform the path-length calibration.

On the other hand, during the second manoeuvre path with the planned rhumb angle $\chi_p = 0$, the spin axis path moves along the local Sun-cone circle and maintains a constant Sun aspect angle during the manoeuvre path, at least nominally, see Figure 1. If the measured final Sun aspect angle turns out to be larger than the planned constant value, we know that the rhumb angle was actually negative instead of 0 (and vice versa).

Therefore, the calibration should assign a negative calibration value to the planned rhumb angle, which is consistent with the minus sign in Eq. (17b). In this case, the Sun-aspect-angle measurements at the start and end of the manoeuvre provide accurate information about the actual rhumb angle, so that in this second manoeuvre path we can achieve the rhumb-angle calibration.

As a further potential advantage of the proposed calibration strategy, we mention that the path-length calibration performed during the first path may benefit the rhumb-angle calibration during the second manoeuvre path. In practice, this means that, instead of using the initially planned thrust level, we employ the improved thrust-level knowledge that resulted from the path-length calibration after completion of the first manoeuvre path.

**Summary of Parameters Used for the Calibrations**

Table 1 summarizes the initial and final designations of the actual, planned, as well as the *measured* rhumb-line Sun angles. Similarly, Table 2 provides the actual, planned, as well as the *calibrated* rhumb-line parameters.

**Table 1. Sun Angle Measurements of Rhumb-Line Manoeuvre**

| Parameter | Actual (unknown) | Target (planned) | Measured | Differences |
|---|---|---|---|---|
| Initial SAA | $\vartheta_i$ | $\vartheta_{i,\,p}$ | $\vartheta_{i,\,m}$ | $\delta\vartheta_i = \vartheta_{i,\,m} - \vartheta_{i,\,p}$ |
| Final SAA | $\vartheta_f$ | $\vartheta_{f,\,p}$ | $\vartheta_{f,\,m}$ | $\delta\vartheta_f = \vartheta_{f,\,m} - \vartheta_{f,\,p}$ |

**Table 2. Calibrations of Rhumb-line Manoeuvre Parameters**

| Parameter | Actual (unknown) | Target (planned) | Calibrated | Calibrations |
|---|---|---|---|---|
| Path length | $\lambda$ | $\lambda_p$ | $\lambda_c$ | $\Delta\lambda = \lambda_c - \lambda_p$ |
| Rhumb angle | $\chi$ | $\chi_p$ | $\chi_c$ | $\Delta\chi = \chi_c - \chi_p$ |

## ERROR ANALYSIS

When recognizing that the *planned* manoeuvre parameters are deterministic variables, we can construct the following expression for the errors in the generalized measurements $y_j$, see Eqs. (10a) and (10f):

$$\Delta y_j = \{\Delta\vartheta_f^{(j)} - \Delta\vartheta_i^{(j)}\} / \lambda_{f,p}^{(j)} = m^{(j)} / \lambda_{f,p}^{(j)}, \quad j = 1,2 \tag{20}$$

The non-italic $\Delta$ appearing here is defined as $\Delta a = a_m - a = \delta a - \Delta a$ and represents the difference between measured and actual variables, i.e. the familiar measurement error.

We assume that the Sun-aspect-angle measurements are independent from each other, which is realistic when we consider random errors. This allows us to calculate the covariance matrix of the measurement vector $\mathbf{y} = (y_1, y_2)^\mathsf{T}$ as follows:

$$cov(\mathbf{y}) = E\{\Delta\mathbf{y} \bullet \Delta\mathbf{y}^\mathsf{T}\} = \sigma^2 \Lambda^{-2}, \text{ with}: \Lambda = \begin{bmatrix} \lambda_{f,p}^{(1)} & 0 \\ 0 & \lambda_{f,p}^{(2)} \end{bmatrix} \tag{21a,b}$$

The errors in the Sun-aspect-angle measurements are known from the observed Sun-sensor measurement performances, i.e. $\sigma = \sqrt{2}\sigma_\vartheta$, see Eq. (7b).

With the help of Eq. (11) we can now calculate the expected errors in the calibrated manoeuvre parameters $\mathbf{x} = (x_1, x_2)^\mathsf{T}$ from Eq. (21) by means of the pseudo-inverse formula:

$$\Delta\mathbf{x} = \left(A^\mathsf{T}A\right)^{-1} A^\mathsf{T}\Delta\mathbf{y} \quad \Rightarrow \tag{22a}$$

$$E\{\Delta\mathbf{x} \bullet \Delta\mathbf{x}^\mathsf{T}\} = \left(A^\mathsf{T}A\right)^{-1} A^\mathsf{T} cov(\mathbf{y}) A \left(A^\mathsf{T}A\right)^{-1} \quad \Rightarrow$$

$$cov(\mathbf{x}) = \sigma^2 \left(A^\mathsf{T}A\right)^{-1} A^\mathsf{T}\Lambda^{-2} A \left(A^\mathsf{T}A\right)^{-1} \tag{22b}$$

with:

$$\left(A^\mathsf{T}A\right)^{-1} = \begin{bmatrix} a_{11}^2 + a_{21}^2 & a_{11}a_{12} + a_{21}a_{22} \\ a_{11}a_{12} + a_{21}a_{22} & a_{12}^2 + a_{22}^2 \end{bmatrix}^{-1} \tag{23}$$

When we consider the special pairs of manoeuvres defined in Eqs. (16), we find that the matrix $(A^\mathsf{T}A)$ and its inverse are equal to the identity matrix in all four cases. Therefore, when adopting one of these four manoeuvre calibration strategies, we find the following expected errors for the calibration parameters in Eq. (22b):

$$cov(\mathbf{x}) = \sigma^2 A^\mathsf{T}\Lambda^{-2} A \tag{24}$$

where the vector $\mathbf{x}$ consists of the two calibration parameters defined in Eqs. (17a,b).

The results in Eqs. (22b) and (24) indicate that the calibration errors are inversely proportional to the respective manoeuvre path-lengths which is intuitively evident. In the particular case when both manoeuvre path-lengths are equal to 1 radian, we see from Eq. (21b) that $\Lambda$ is reduced to the identity matrix. Therefore, only the $\sigma^2$ term is left on the right-hand side of Eq. (24) and the calibration errors of both path-length and rhumb angle are equal to $\sigma \approx 0.0014$ deg.

In practice there will be a number of systematic errors (i.e., biases) that may be significantly larger than the random errors discussed here. In particular, spin-rate changes and variations in the thrust levels during and in-between the manoeuvre paths are usually the main error sources.

## APPLICATION TO CONTOUR

Two dedicated calibration manoeuvres were performed by the CONTOUR satellite in summer 2002 to achieve the calibration of the manoeuvre path-length (i.e., thrust level) and the rhumb angle (i.e., centroid time), see Reference 1. The strategy outlined above was used for this purpose, in particular the pair of orthogonal manoeuvre paths proposed in Eqs. (16).

The two manoeuvre paths selected for CONTOUR were incorporated in the 180-deg flip manoeuvre needed to establish the correct attitude for executing an orbit correction manoeuvre at the second perigee. The calibrations took advantage of the accurate Sun-aspect angle measurements generated by the Sun-sensor. No other sensor measurements were used nor needed.

The first manoeuvre path aimed at achieving the thrust-level calibration. It used a manoeuvre path that was headed normal to the local Sun cone. Therefore, the Sun sensor was able to accurately measure the achieved path-length.

The second manoeuvre path was used to perform the calibration of the rhumb angle, i.e. the effective centroid time of the thrust pulses. It used a nominal path along the local Sun-cone circle so that the Sun sensor could accurately measure the deviation from this path, i.e. the rhumb angle. As a result of these two calibration manoeuvres (plus a diligent accounting for spin rate effects), CONTOUR's first 180º flip manoeuvre achieved its required target attitude within 3 deg[1].

Figure 3 gives a visualization of the 180-deg flip manoeuvre path in the form of a Mercator projection showing the path of the attitude unit-vector traced on the unit-sphere. The complete manouevre consists of 4 manoeuvre paths, each with its specific path-length and rhumb angle.

The first two shorter paths are dedicated to the calibration objectives and the following two larger paths of about 64 deg lengths complete the 180-deg flip manoeuvre. The interruption in the middle was introduced to be able to correct for any observed spin changes during this very long manoeuvre. The five attitude orientations at the start and end of the four manoeuvre paths are identified by three parameters (RA, DE) / SAA, denoting (Right Ascension, DEclination) / Sun Aspect Angle, respectively.

The nominal first path has a length of about 19 deg and a rhumb angle of +90 deg. Thus, the spin-axis attitude moves nominally along a meridian circle in the direction towards the Sun. This results in a pure (at least nominally) Sun angle change so we can achieve a very precise calibration of the manoeuvre path-length on the basis of the measured change in Sun aspect angle.

The second manoeuvre path is about 57 deg long and follows the direction normal to that of the first path. The rhumb angle is now 180 deg with the attitude moving along the Sun cone at a nominally constant Sun aspect angle. Therefore, any observed change in Sun aspect angle over this manoeuvre path points to a rhumb-angle error and can be used for its calibration.

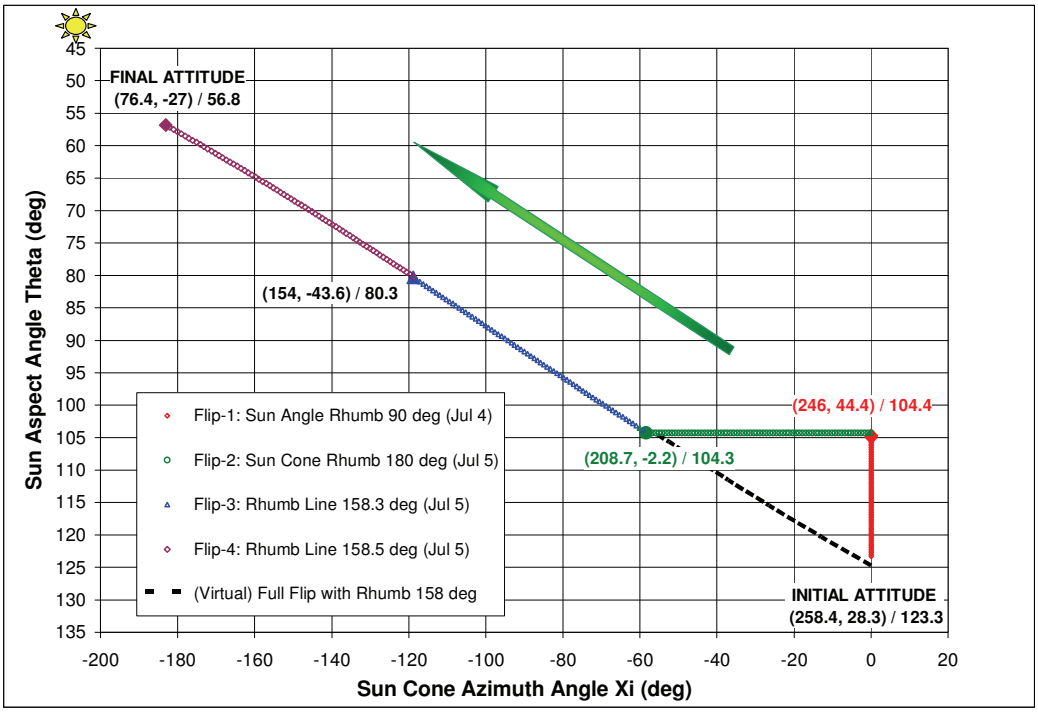


**Figure 3 – Visualization of CONTOUR's 180-deg Rhumb-Line Manoeuvres in July 2002**

## CONCLUSION

The paper presents the principles and technical details of an efficient practical calibration technique for rhumb-line attitude control manoeuvres of spin-stabilized satellites. The strategy is based on common V-slit Sun sensor measurements only. By using two independent manoeuvre paths we can achieve accurate calibration of both the manoeuvre path-length and rhumb angle.

The proposed technique was actually successfully implemented and validated in-flight by the CONTOUR satellite in summer 2002 as an integral part of a 180-deg flip manoeuvre execution. The final attitude error at the end of the complete manoeuvre was below 3 deg.

## APPENDIX: CALIBRATIONS OF MULTIPLE MANOEUVRES

Here we consider the stuation when we have an arbitrary number of $n$ (larger than 2) independent manoeuvre paths that we want to utilize for the calibrations of the rhumb-line path-lengths and the rhumb angles.

This leads to a more general over-determined system of equations that can be analyzed by using the same relationship as given in Eq. (11) but with $n \geq 2$ measurements of the vector $\mathbf{y}$:

$$\mathbf{y} = A\mathbf{x} + \mathbf{m} \tag{A1}$$

with:

$$\mathbf{y} = \begin{pmatrix} y_1 \\ y_2 \\ \dots \\ y_n \end{pmatrix}; \quad A = \begin{bmatrix} a_{11} & a_{12} \\ a_{21} & a_{22} \\ & \dots \\ a_{n1} & a_{n2} \end{bmatrix}; \quad \mathbf{m} = \begin{pmatrix} m_1 \\ m_2 \\ \dots \\ m_n \end{pmatrix} \tag{A2a-c}$$

The optimal calibration parameters are provided by the least-square solution of this system:

$$\hat{\mathbf{x}} = \left(A^{\mathsf{T}} A\right)^{-1} A^{\mathsf{T}} \mathbf{y} \tag{A3}$$

After substituting the relevant rhumb-line matrix elements $a_{jk}$ with $j = 1, 2, \ldots, n$; $k = 1, 2$ of the $n$ manoeuvre paths from Eqs. (10d,e) into Eq. (A3) we obtain:

$$A^T A = \sum_{j=1}^{n} \begin{bmatrix} \sin^2 \chi_p^{(j)} & \sin \chi_p^{(j)} \cos \chi_p^{(j)} \\ \sin^2 \chi_p^{(j)} \cos \chi_p^{(j)} & \cos^2 \chi_p^{(j)} \end{bmatrix} \tag{A4}$$

and the explicit calibration follows from Eq. (A3):

$$\hat{\mathbf{x}} = -\left\{ \sum_{j=1}^{n} \begin{bmatrix} \sin^2 \chi_p^{(j)} & \sin \chi_p^{(j)} \cos \chi_p^{(j)} \\ \sin^2 \chi_p^{(j)} \cos \chi_p^{(j)} & \cos^2 \chi_p^{(j)} \end{bmatrix} \right\}^{-1} \sum_{j=1}^{n} y_j \begin{pmatrix} \sin \chi_p^{(j)} \\ \cos \chi_p^{(j)} \end{pmatrix} \tag{A5}$$

We can now perform the same error analysis as in Eqs. (20) - (24) and write the expected error in a similar same form as in Eq. (22a):

$$\Delta \mathbf{x} = \hat{\mathbf{x}} - \mathbf{x} = \left(A^{\mathsf{T}} A\right)^{-1} A^{\mathsf{T}} \Delta \mathbf{y} \tag{A6}$$

with covariance matrices:

$$cov(\mathbf{y}) = E\{\Delta \mathbf{y} \bullet \Delta \mathbf{y}^{\mathsf{T}}\} = \sigma^2 \Lambda_n^{-2}, \text{ with: } \Lambda_n = \begin{bmatrix} \lambda_{f,p}^{(1)} & 0 & \dots & 0 \\ 0 & \lambda_{f,p}^{(2)} & \dots & 0 \\ & \dots\dots\dots & & \\ 0 & \dots & & \lambda_{f,p}^{(n)} \end{bmatrix} \tag{A7a}$$

and:

$$cov(\mathbf{x}) = \sigma^2 \left(A^{\mathsf{T}} A\right)^{-1} A^{\mathsf{T}} \Lambda_n^{-2} A \left(A^{\mathsf{T}} A\right)^{-1} \tag{A7b}$$

This result is a generalization of the result in Eq. (22b) and is valid for any type of $n \geq 2$ independent manoeuvres, each with its own path-length and rhumb angles and associated errors.

## REFERENCES


[1] van der Ha, J., Rogers, G., Dellinger, W., and Stratton, J., "CONTOUR Phasing Orbits: Attitude Determination & Control Concepts and Flight Results," *Advances in the Astronautical Sciences,* Vol. 114, Part II, 2003, pp. 767-781.

[2] van der Ha, J. C., "Models for Rhumb-Line Attitude Manoeuvres and Error Propagation Effects," *Journal of Guidance, Control, and Dynamics*, Vol. 29, No. 6, 2006, pp. 1384-1394.

[3] van der Ha, J. C., "Progress in Satellite Attitude Determination and Control," *JSASS Aeronautical and Space Sciences Japan Journal*, Vol. 57, No. 666, July 2009, pp. 1-8.

[4] van der Ha, J. C., "Performance of Spin Axis Attitude Estimation Algorithms with Real Data," *19-th AAS Space Flight Mechanics Symposium*, Savannah, GA, February 8-12, 2009, Paper AAS-09-127; *Journal of Guidance, Control, and Dynamics*, Vol. 33, No. 3, May-June 2010, in print.